PD-1 blockade inhibits osteoclast formation and murine bone cancer pain

Kaiyuan Wang, Yun Gu, Yihan Liao, Sangsu Bang, Christopher R. Donnelly, Ouyang Chen, Xueshu Tao, Anthony J. Mirando, Matthew J. Hilton, and Ru-Rong Ji

Supplementary Methods

Supplementary figures (15)

Supplementary tables (2)

Supplementary Methods

Hematoxylin and Eosin staining

Paraffin sections were baked at 60˚C for 2 hours, then deparaffinized, rehydrated and stained. After dehydration and clearance with HistoClear (Electron Microscopy Sciences, Hatfield, PA), slides were mounted with a resinous mounting medium and viewed under a Leica Q500MC microscope with a digital camera (×2). Tumor and the total marrow areas between the epiphyseal plates within the femur were measured using image analysis software (Image J, NIH). Femoral tumor burden was evaluated by the percentage of intramedullary space occupied by the tumor (1).

In vivo TRAP and ALP staining

Modified TRAP and ALP staining of paraffin femur sections were performed with TRAP kits (Fast Red TR/Naphthol AS-MX, Sigma, St. Louis, MO) for osteoclasts and NBT/BCIP (Thermo Scientific) for osteoblasts. Bone static histomorphometric analyses for osteoclast surface (the percent of trabecular bone surface covered by osteoclasts, Oc.S/BS) and osteoblast number (osteoblast number per trabecular bone surface, Ob.N/BS) were conducted using Image J (NIH) under a Leica Q500MC microscope with a 5x digital camera. For all groups, osteoclasts, osteoblasts and trabecular bone were counted at the metaphysis of the femur (1500 μm proximal to the distal growth plate), as bone destruction occurs mainly in this area (1, 2). Four to ten continuous sections were used for quantification per animal.

Immunohistochemistry

After being removed of paraffin and rehydrated the femur sections were submerged in pre-heated antigen retrieval solution and boiled for 15 min. The sections were blocked with 10% normal donkey serum for 1 h at room temperature (RT). The sections were further incubated with rabbit anti-PD-L1 antibody (1:500, Abcam, #ab205921) or rabbit anti-PD-1 antibody (1:500, Sigma, #PRS4065) in 5% normal goat serum/PBS overnight at 4 °C. The sections were incubated with

Cy3-labeled anti-rabbit secondary antibody (1:500, Abcam, #ab6939) for 2 h at RT. For PD-1 and PD-L1 double immunostaining, we used the rabbit anti-PD-L1 antibody (1:500, Abcam, #ab205921) and cy5-conjugated PD-1 antibody (1:500, Bristol-Myers Squibb, #NDC 0003-3772-11). Fluorescence images were obtained with a Nikon fluorescence microscope (Nikon DS-Ti, Tokyo, Japan).

Bone marrow collection

Mice were humanely euthanized and the femora were removed carefully and placed on ice. We used a tweezer to dissociate the distal epiphysis from femoral shaft gently. The proximal end of the femur was cut by a scalpel blade. We then inserted a 25-gauge needle into the distal end of the femur and injected 1 ml cold PBS or α-MEM (Gibco, Thermo Fisher Scientific) to lightly press down on the plunger to force the bone marrow out into a 1.5 ml centrifuge tube. We then flushed twice and inverted the bone to flush twice from the proximal end. Bone marrow was harvested through centrifugation at 800g for 5 minutes at 4 °C for subsequent detections or cell cultures.

ELISA

Mouse PD-L1 ELISA kit was purchased from US Biological (Catalog: 027620). Mouse CCL2/JE/MCP-1 ELISA Kit was purchased from R&D system (Catalog: MJE00B). Mouse CTX-I ELISA kit (Catalog: AC-06F1) and mouse PINP ELISA kit (Catalog: AC-33F1) were from Immunodiagnostic Systems. ELISA was performed using culture medium, serum, bone marrow lysates and exosomes from serum. Serum was obtained from whole blood, collected from a submandibular vein. After 60 min at room temperature, the clot was removed in a refrigerated centrifuge at 3,000 × g for 10 min to collect the supernatant (serum). ELISA was conducted strictly according to the manufacturer's instructions. The standard curve was included in each experiment.

Western blot

Bone marrow, tumor or para-tumor tissues and BMDM were homogenized in a lysis buffer

containing protease and phosphatase inhibitors at 4°C for 30 min. We loaded 50-100 μg protein for each lane and separated proteins by SDS-PAGE gel (4-20%; Bio-Rad). After the transfer, the blots were incubated overnight at 4°C with primary antibodies against PD-L1 (1:500, rabbit, Abcam, #ab213480), as well as p-ERK, ERK, p-JNK, JNK, p-p38, and p38 (1:1000, rabbit, Cell Signaling Technology, #9101S, #9102S, #4668S, #9252S, #9211S, and #8690S, respectively). For the loading control, the blots were probed with GAPDH antibody (1:2,000, rabbit, Cell Signaling Technology, #2118S). The blots were then incubated with an HRP-conjugated secondary antibody and developed in ECL solution (Pierce, Thermo Fisher Scientific). Chemiluminescence signal was revealed by Bio-Rad ChemiDoc XRS for 1 to 10 minutes. Specific bands were evaluated according to apparent molecular sizes. Full gels of the represented blots were included in Supplemental Figure 15.

Cytokine array

The mouse cytokine assay kit was purchased form R & D Systems (Catalog: ARY006). The assay was performed according to the manufacturer's protocol. Briefly, the array membranes were incubated with cell culture medium from BMDM together with detection antibody cocktail overnight. Then the membranes were incubated for 30 min with Streptavidin-HRP and were exposed to X-ray film for 1-10 minutes after development with Chemi Reagent Mix.

***In situ* hybridization**

Mice were deeply anesthetized with isoflurane and transcardially perfused with PBS followed by 4% paraformaldehyde/1.5% picric acid. L4-L5 DRGs were removed and post-fixed overnight at 4°C. DRG sections were cut (14 μm) in a cryostat. Each slide contained both ipsilateral and contralateral DRG sections to control for variability in staining. *In situ* hybridization was performed using the RNAscope system (Advanced Cell Diagnostics) according to the manufacturer's protocol. We used a probe directed against murine *Ccr2* (NM_009915.2, #501681). Immunostaining was performed overnight at 4°C for the pan-neuronal marker TuJ1 (Sigma,

#T8578) and labeled with secondary antibody (donkey anti-mouse-633, Biotium, #20124). Images were captured using an epifluorescent microscope (Nikon Eclipse NiE) with the same acquisition settings for all animals. The number of *Ccr2*$^{+}$ mRNA puncta per neuron was quantified in at least 3 sections per DRG for each animal by an experimenter blinded to the conditions.

Exosome isolation

The serum exosomes were collected using Total Exosome Isolation Reagent (Invitrogen™, Catalog: 4478360) and incubated at 4°C for 30 minutes. After incubation, we centrifuged the sample at 15,000 × g for 10 minutes at room temperature. The collected exosome samples were then used for flow cytometry analysis.

Antibody labeling and in vivo detection of nivolumab

To detect the serum antibody levels, nivolumab and human IgG were conjugated (0.1 mg biotin per mg antibody) by an EZ-LinkTM Sulfo-NHS-biotiylation kit (Thermo Scientific), according to the manufacturer's instructions. The mixture was incubated overnight at 4 °C. To visualize the antibody binding to cells or animal tissues, nivolumab (1 mg) was conjugated with Vivo-680 (10 μg) dye in 0.1 mol/L sodium bicarbonate buffer overnight at 4 °C, according to the manufacturer's instructions (PerkinElmer). Non-binding biotin or Vivo-680 was removed by dialysis (4 °C, 24 h) for salt exchange using a membrane with a 10 kDa cut-off (Sigma). Specific antibody was predicated with gel-filtration filter and then dilated with PBS. The quantity of labeled antibody was calculated by Nano-drop. To detect the nivolumab levels, the serum samples (10 μL) were incubated in a streptavidin-coated plate (96-well, Thermo Scientific) at RT for 2 h. The binding antibody complex was detected by HRP-conjugated human IgG antibody (diluted 1:1000 in PBST buffer, Thermo Scientific). The plates were then incubated with 100 μL tetramethylbenzidine (TMB)-based substrate (KPL Inc.). After 20 min of incubation at RT, 100 μL of 1 mol/L HCl were added to stop the reaction. The resulting color reaction was measured at 450 nm with an ELISA reader (Bio-Rad).

In vivo fluorescence imaging

On day 8 after LLC inoculation into the left femur of mice, we injured 10 mg/kg of Vivo-680-tagged nivolumab via tail vein. Mice were then subjected to NIRF imaging. At different time points post antibody injection, mice were scanned using a PerkinElmer VisEn FMT2500LX imaging system with an excitation bandpass filter at 670 nm and emission at 745 nm under isoflurane anesthesia. The area intensity of fluorescence was measured by TrueQuant Imaging Software (PerkinElmer).

References

1. Lozano-Ondoua AN, et al. Disease modification of breast cancer-induced bone remodeling by cannabinoid 2 receptor agonists. *J Bone Miner Res.* 2013;28(1):92-107.
2. Honore P, et al. Osteoprotegerin blocks bone cancer-induced skeletal destruction, skeletal pain and pain-related neurochemical reorganization of the spinal cord. *Nat Med.* 2000;6(5):521-528.

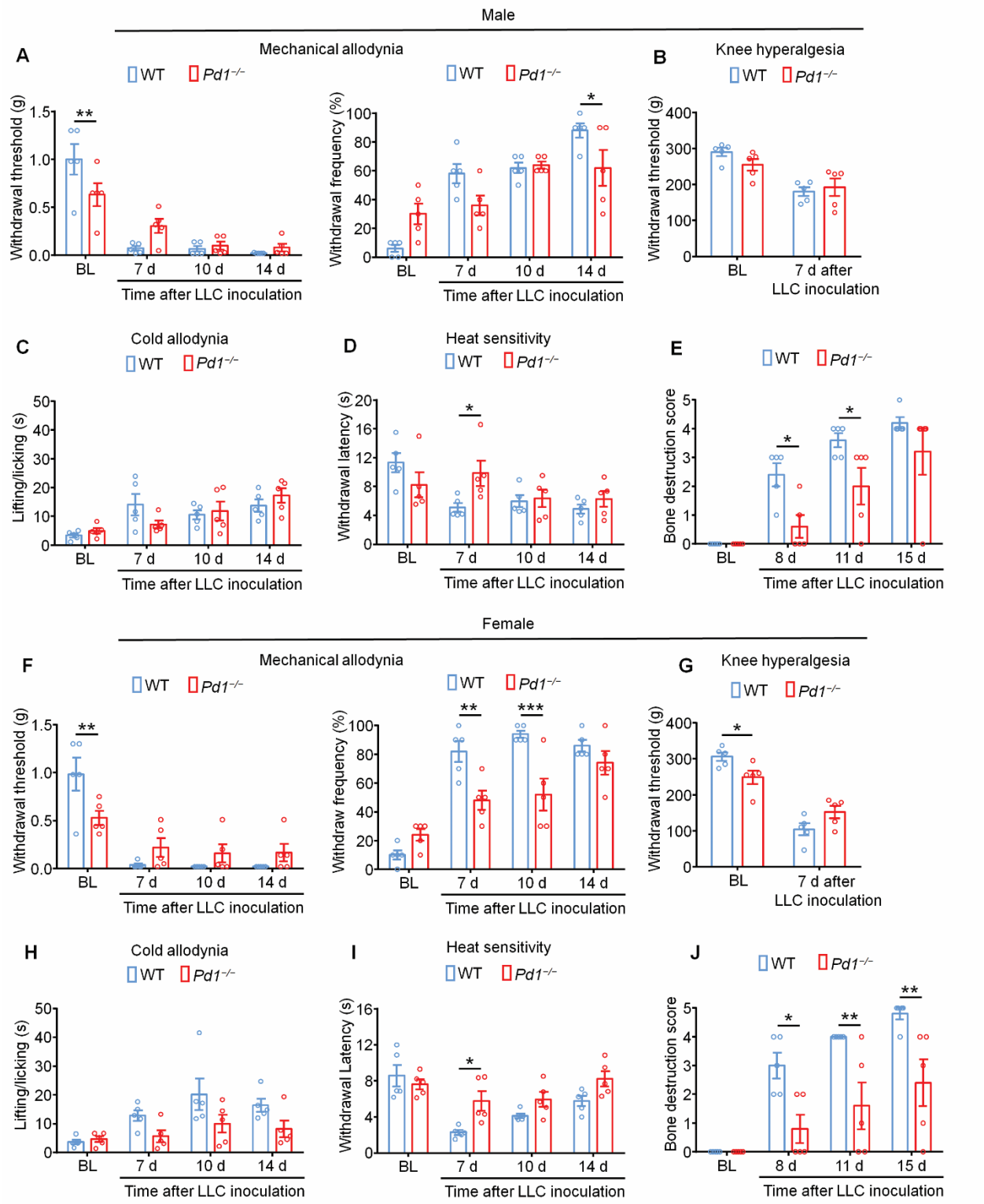

Supplementary Figure 1. Reduction of cancer-induced bone pain and bone destruction in both male (A-E) and female (F-J) *Pd1*$^{-/-}$ mice. (A-E) LLC-induced mechanical allodynia (A), knee hyperalgesia (B), cold allodynia (C), heat hyperalgesia (D) and bone destruction score (E) in male WT and *Pd1*$^{-/-}$ mice. n = 5 male mice per group. (F-J) LLC-induced mechanical allodynia

(F), knee hyperalgesia (G), cold allodynia (H), heat hyperalgesia (I) and bone destruction score (J) in male WT and *Pd1*$^{-/-}$ mice. n = 5 female mice per group. Data are Mean ± SEM. **P* < 0.05, ***P* < 0.01 and ****P* < 0.001, repeated-measures two-way ANOVA with Bonferroni's *post hoc* test. BL, baseline.

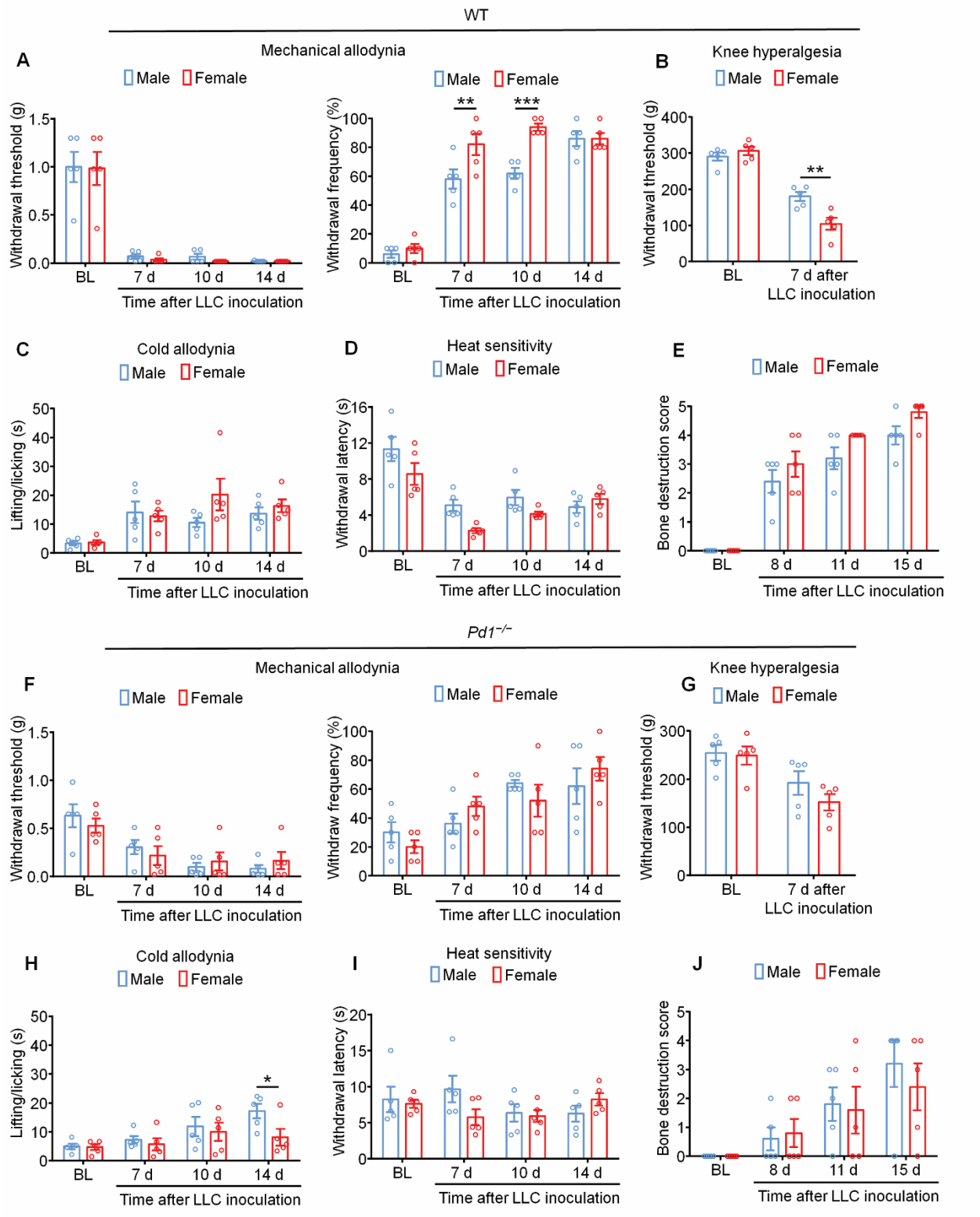

Supplementary Figure 2. No obvious sexual differences in cancer-induced bone pain and bone destruction in WT or *Pd1*$^{-/-}$ mice. (A-E) Comparison of bone pain and bone destruction between male and female WT mice. Although female WT mice had higher withdrawal frequency

from Von Frey test (A) and more knee hyperalgesia (B) compared with male WT mice, they showed no statistical differences from WT males in cold allodynia (C), heat hyperalgesia (D) and bone destruction (E). (n = 5 per group). (F-J) Comparison of bone pain and bone destruction between male and female KO mice. No statistical differences were found in mechanical allodynia (F), knee hyperalgesia (G), heat hyperalgesia (I) and bone destruction score (J) between male and female *Pd1*$^{-/-}$ mice, except for cold allodynia (H) at day 14. n = 5 mice per group. Mean ± SEM. **P* < 0.05, ***P* < 0.01 and ****P* < 0.001, repeated-measures two-way ANOVA with Bonferroni's *post hoc* test. BL, baseline.

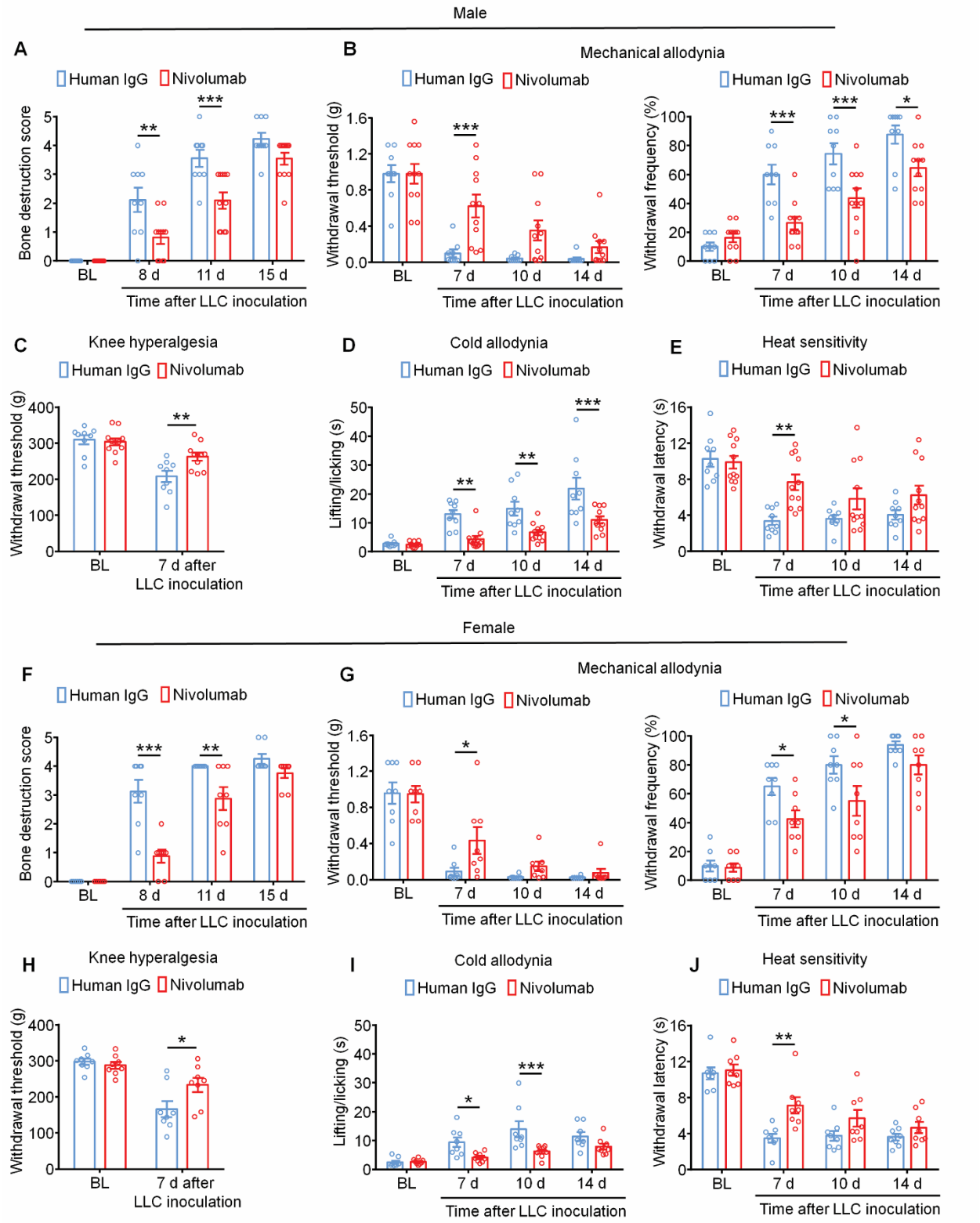

Supplementary Figure 3. Nivolumab treatment is effective in both male and female mice with LLC inoculation. (A-E) Nivolumab treatment (i.v., 5 x 10 mg/kg) attenuated bone destruction (A), mechanical allodynia (B), knee hyperalgesia (C), cold allodynia (D) and heat hyperalgesia

(E) after LLC inoculation in male mice. n = 9 or 11 male mice per group. (F-J) Nivolumab treatment (i.v., 5 x 10 mg/kg) reduced bone destruction (F), mechanical allodynia (G), knee hyperalgesia (H), cold allodynia (I) and heat hyperalgesia (J) after LLC inoculation in female mice. n = 8 female mice per group. Mean ± SEM. *$P < 0.05$, **$P < 0.01$ and ***$P < 0.001$, repeated-measures two-way ANOVA with Bonferroni's *post hoc* test. BL, baseline.

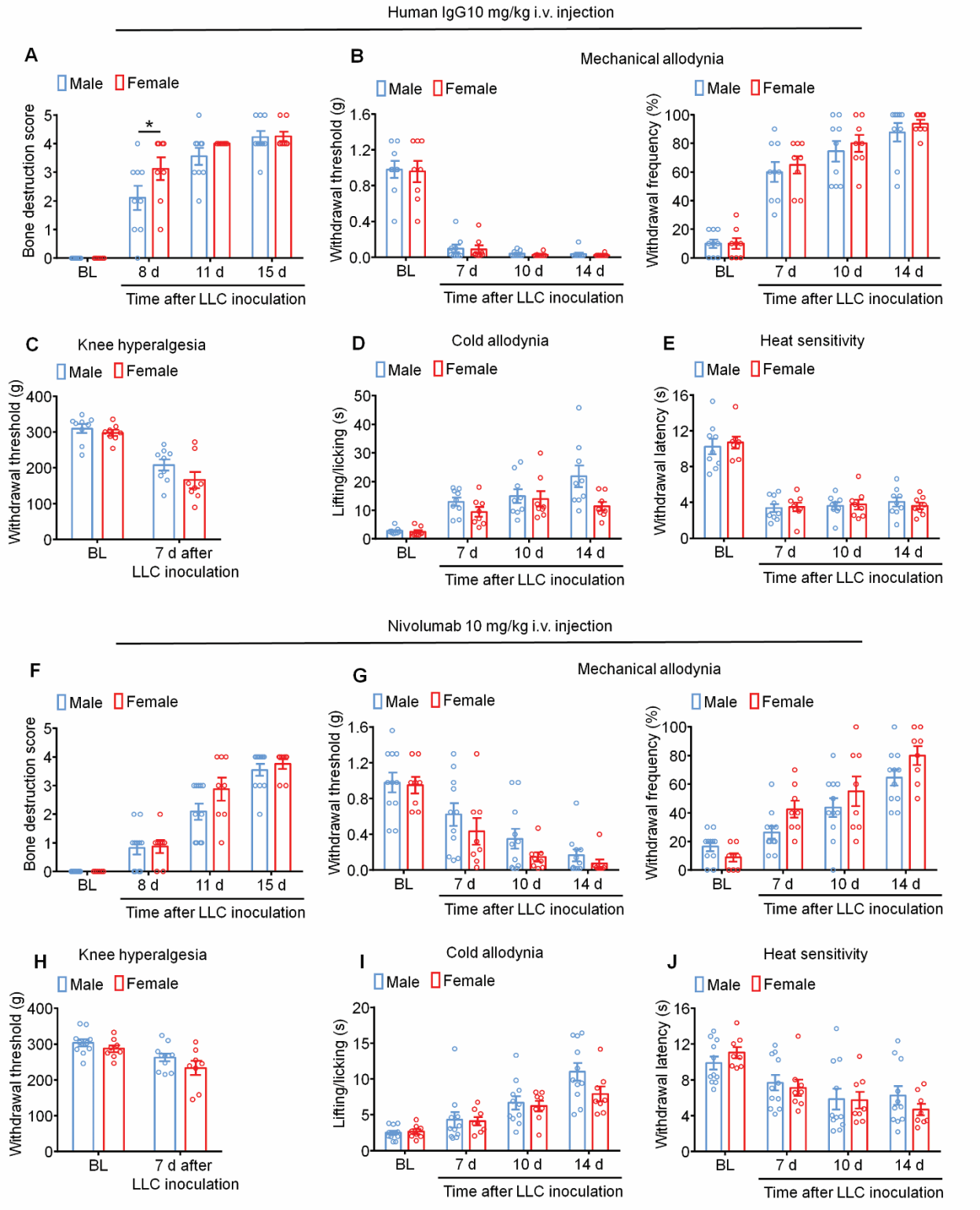

Supplementary Figure 4. No sexual differences in cancer-induced bone pain and bone destruction following control IgG or nivolumab treatment. (A-E) No sex difference is found in bone destruction score (A), mechanical allodynia (B), knee hyperalgesia (C), cold allodynia (D)

and heat hyperalgesia (E) between male and female mice treated with human IgG (i.v., 5 x 10 mg/kg). n = 8 or 9 mice per group. (F-J) No sex difference is found in bone destruction score (F), mechanical allodynia (G), knee hyperalgesia (H), cold allodynia (I) and heat hyperalgesia (J) between male and female mice treated with nivolumab (n = 8 or 11 per group). Data are Mean ± SEM. Repeated-measures two-way ANOVA with Bonferroni's *post hoc* test. BL, baseline.

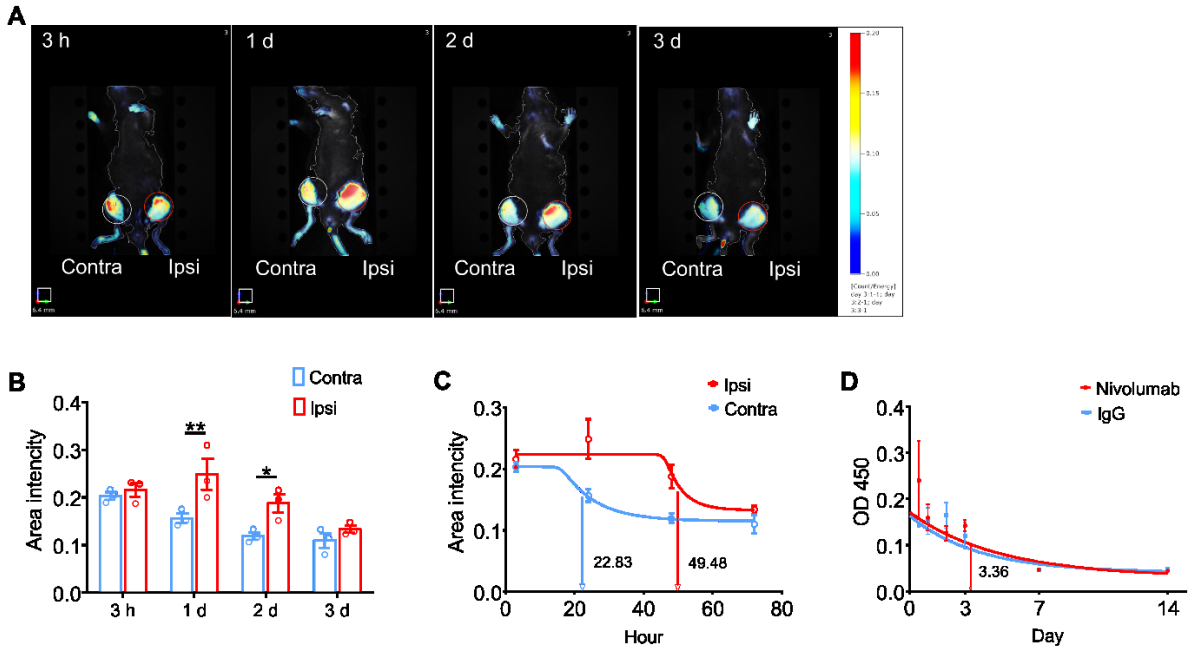

Supplementary Figure 5. Detection of nivolumab metabolism in C57 BL/6 mice. (A) Whole animals imaging showing the distribution of Vivo-680 tagged nivolumab in ipsilateral and contralateral femur on 3 h, 1 d, 2 d and 3 d after i.v. injection of the labeled nivolumab (10 mg/kg). (B and C) Quantifications of area intensity in A. n = 3 male mice per group. (D) OD values of labeled nivolumab and human IgG detected in serum at 3 h, 1 d, 2 d, 3 d, 7 d and 14 d after nivolumab or human IgG injection (i.v., n = 6 male mice per group). The half-life of nivolumab is 3.36 days in mouse serum. Data are Mean ± SEM. *P<0.05, **P < 0.01, repeated-measures two-way ANOVA with Bonferroni's *post hoc* test.

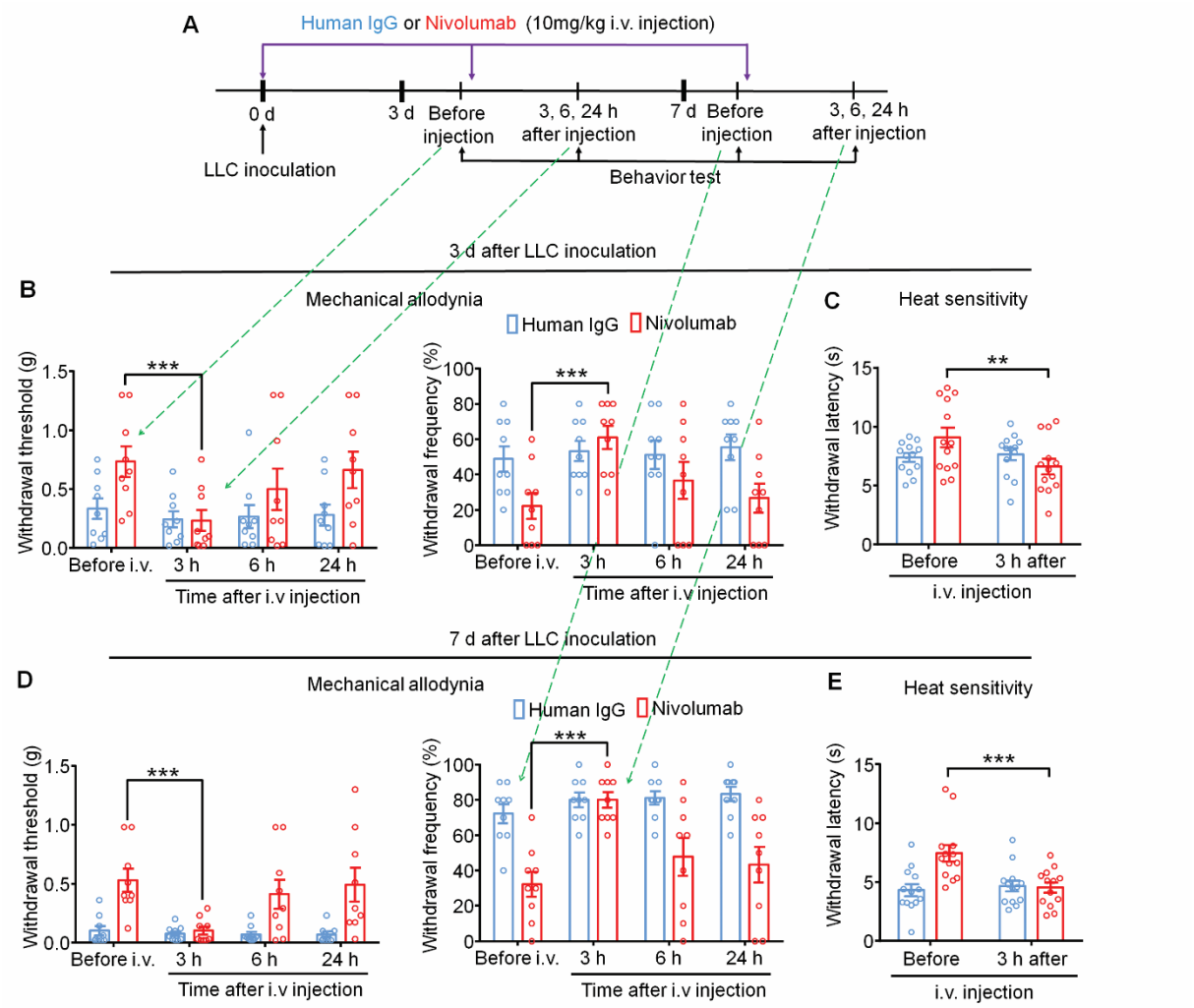

Supplementary Figure 6. Nivolumab transiently increases pain sensitivity 3 h after IV injection. (A) Experimental diagram showing the timeline of i.v. injection of human IgG or nivolumab and behavior tests. (B and C) Nivolumab evokes rapid mechanical allodynia (B) and heat hyperalgesia (C) 3 h after i.v. injection on day 3 after LLC inoculation (n = 9-13 mice per group). (D and E) Nivolumab produces rapid mechanical allodynia (D) and heat hyperalgesia (E) 3 h after i.v. injection on day 7 after LLC inoculation. n = 9-13 mice per group, either sex. Data are Mean ± SEM. $^{**}P < 0.01$ and $^{***}P < 0.001$, two-way ANOVA with Bonferroni's *post hoc* test.

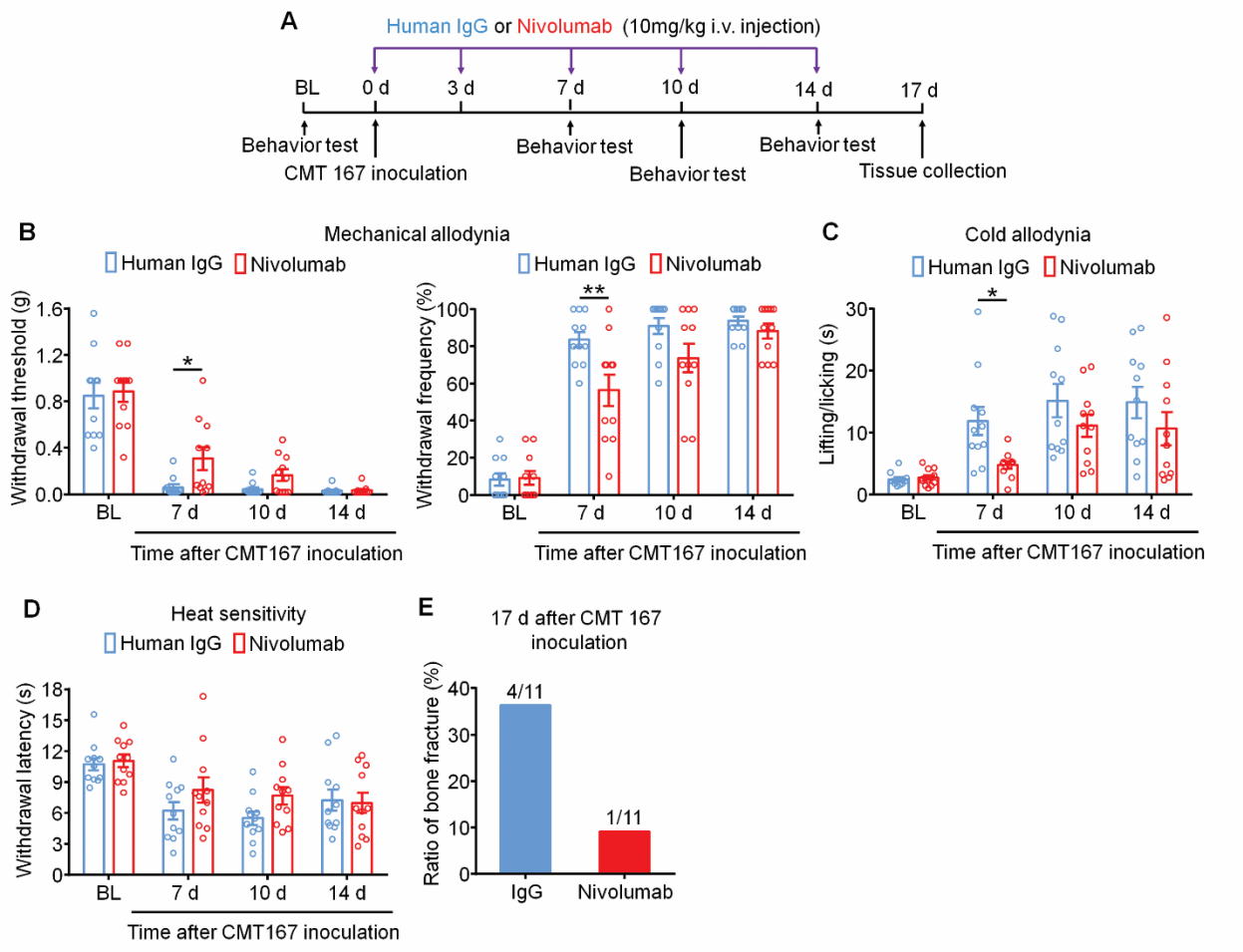

Supplementary Figure 7. Effects of nivolumab treatment on CMT 167 induced bone cancer pain and bone fracture. (A) Experimental diagram showing the time course of i.v. injection of human IgG or nivolumab and behavior tests. (B, C) Nivolumab treatment reduces mechanical allodynia in von Frey test (B) and cold allodynia in acetone test (C) on day 7 after tumor inoculation. n = 11 mice per group. (D) No effect of nivolumab on heat hyperalgesia in Hargreaves test. n = 11 mice per group. (E) Ratio of bone fracture in nivolumab and human IgG treated mice on day 17 after CMT167 inoculation. n = 11 mice per group. Data are Mean ± SEM. **P* < 0.05 and ***P* < 0.01, repeated-measures two-way ANOVA with Bonferroni's *post hoc* test (B-D); Fisher's exact test (E). BL, baseline.

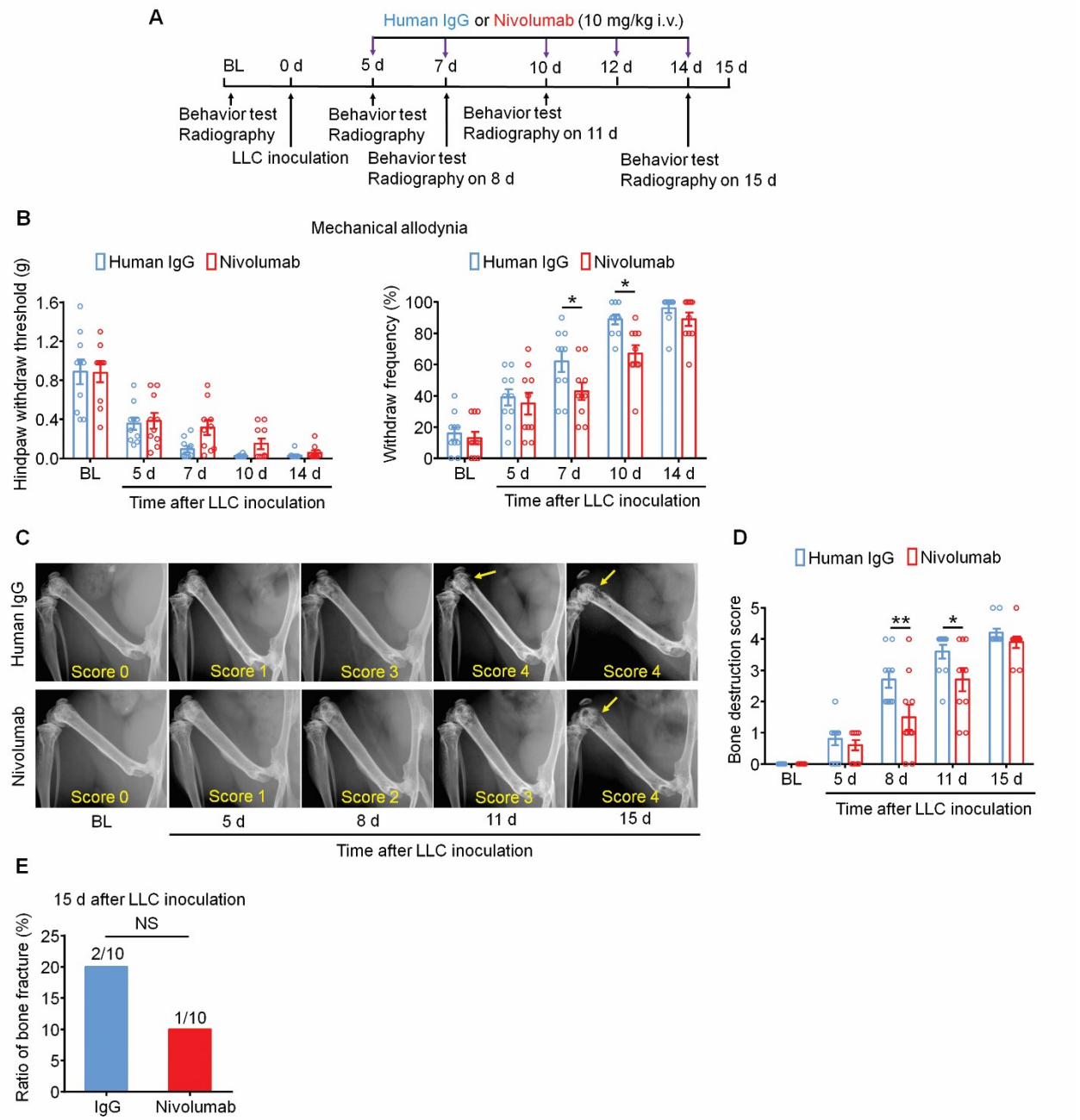

Supplementary Figure 8. Post-treatment of nivolumab reduces bone pain and bone destruction after LLC inoculation. (A) Experimental diagram showing the time course of i.v. injection of human IgG or nivolumab, behavior tests, and radiography. Note nivolumab treatment (5 x 10 mg/kg) started 5 days after LLC inoculation when cancer pain is established. (B) Nivolumab treatment reduces mechanical allodynia in von Frey test. n = 10 mice per group. (C) Radiographs of tumor-bearing femora of IgG or nivolumab treated mice. Bone destruction score is shown at the bottom of each graph and arrows indicated lesions with bone destruction scores over 3. (D) Quantification of bone destruction score. n = 10 mice per group. (E) Effect of nivolumab on bone fracture on day 15 post tumor implantation. Data are Mean ± SEM. *$P < 0.05$

and **$P < 0.01$, repeated-measures two-way ANOVA with Bonferroni's *post hoc* test (B and D); Fisher's exact test (E). BL, baseline; NS, no significance.

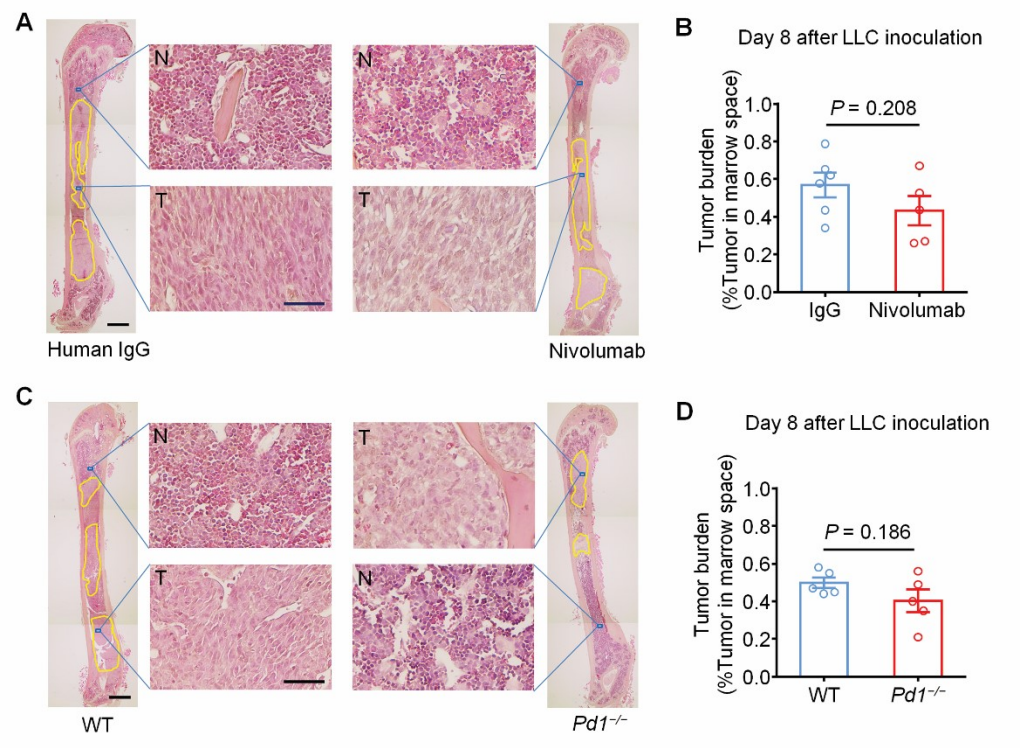

Supplementary Figure 9. Nivolumab treatment fails to reduce tumor burden following LLC inoculation. (A) Hematoxylin and eosin (H & E) images of whole femur sections of human IgG and nivolumab treated mice. Area labeled within yellow line denotes tumor tissue. Scale bar, 1000 µm. Enlarged boxes illustrate normal bone marrow cells (N) and tumor cells (T). Note tumor cells have larger and irregular nuclei. Scale bar, 50 µm. (B) Analysis of tumor growth within the intramedullary space of the femur shows unaltered tumor growth on day 8 post-tumor inoculation in nivolumab treated mice. n = 5-6 male mice per group. (C and D) H & E images and quantification of tumor growth in tumor bearing femora on day 8 after LLC inoculation in WT and *Pd1*$^{-/-}$ mice (n = 5 male mice per group). Scale bar in whole femur, 1000 µm. Scale bar in enlarged box, 50 µm Data are Mean ± SEM, two-tailed Student's *t*-test.

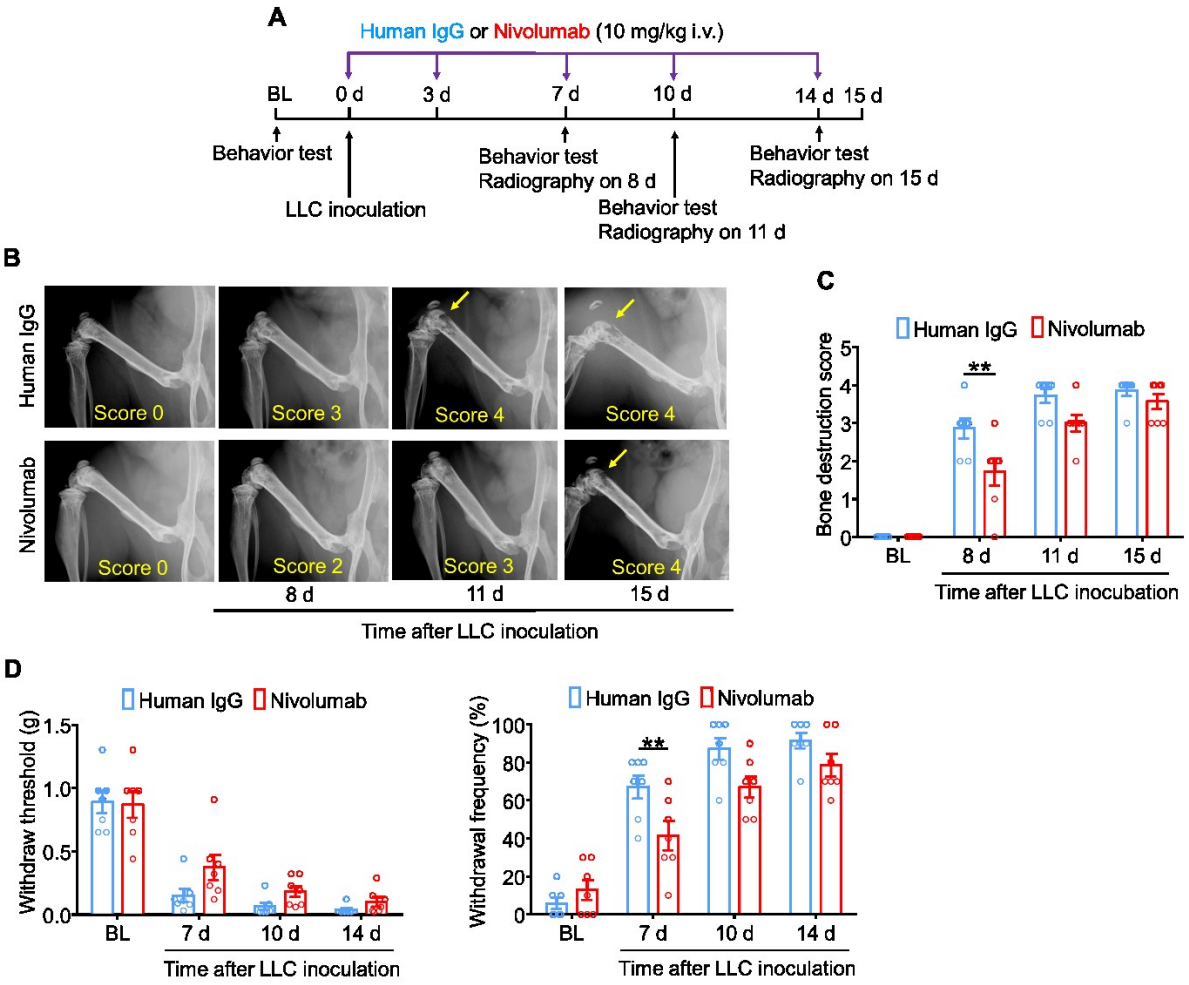

Supplementary Figure 10. Effects of nivolumab treatment on bone destruction and cancer induced bone pain in *Rag1*$^{-/-}$ mice. (A) Experimental diagram showing the time course of i.v. injection of human IgG or nivolumab, behavior tests, and radiography. (B) Representative radiographs of tumor-bearing femora of IgG or nivolumab treated mice. Bone destruction score is shown at the bottom of each graph and arrows indicat lesions with bone destruction score over 3. (C) Quantification of bone destruction score. n = 7 mice per group. (D) Nivolumab treatment attenuates mechanical allodynia on day 7 after tumor inoculation in von Frey test. n = 7 mice per group. Data are Mean ± SEM. $^{**}P < 0.01$, repeated-measures two-way ANOVA with Bonferroni's *post hoc* test. BL, baseline.

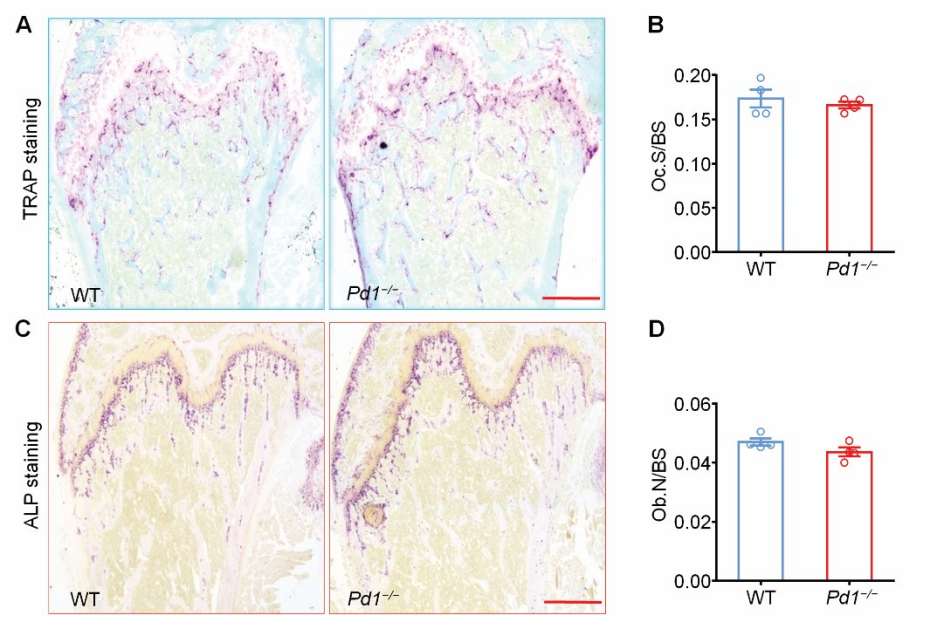

Supplementary Figure 11. Osteoclast and osteoblast number in naïve WT and *Pd1*$^{-/-}$ mice. (A and B) Representative images (A) and quantification (B) of TRAP staining showing no statistical difference between naïve WT and *Pd1*$^{-/-}$ mice. n = 4 male mice per group, and 4-10 sections were collected per femur. Scale bar, 500 μm. (C and D) Representative images (C) and quantification (D) of ALP staining showing no difference between 2 groups. n = 4 male mice per group, and 4-10 sections were collected per femur. Scale bar, 500 μm. Data are Mean ± SEM, two-tailed Student's *t*-test. Oc.S/BS: Osteoclast surface per trabecular bone surface; Ob.N/BS, Osteoblast number per trabecular bone surface.

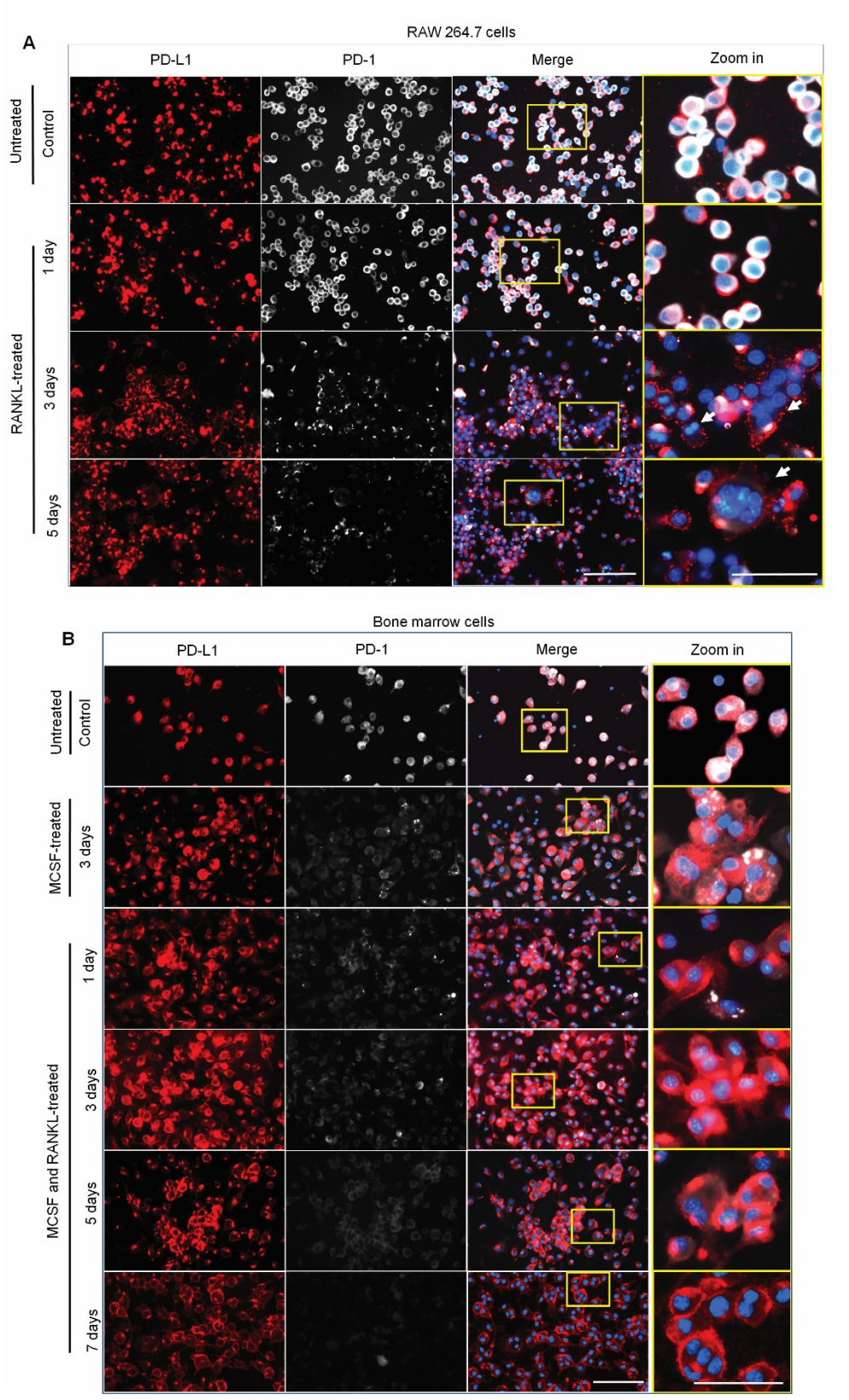

Supplementary Figure 12. Time-dependent expression of PD-L1 and PD-1 during the

differentiation of RAW 264.7 cells and mouse bone marrow cells into osteoclast-like cells induced by RANKL. (A) Double immunostaining of PD-L1 (red) and PD-1 (white) in RAW 264.7 cells cultured without (control) and with RANKL (1, 3 and 5 days after RANKL incubation). Note during the induction of osteoclasts, PD-1 expression is gradually lost. Scale bar, 100 μm. Enlarged box show the high-magnification merged images of PD-L1 and PD-1 staining during osteoclastogenesis. Scale bar, 50 μm. **(B)** PD-L1 (red) and PD-1 (white) staining in isolated bone marrow cells cultured without MCSF and RANKL (control) and in bone marrow cells co-cultured with MCSF and RANKL at different time points. Note a loss of PD-1 expression during the induction of osteoclasts. Scale bar, 100 μm. Enlarged box show the high-magnification merged images of PD-L1 and PD-1 staining during osteoclastogenesis. Scale bar, 50 μm.

A

	1, 2	3, 4	5, 6	7, 8	9, 10	11, 12	13, 14	15, 16	17, 18	19, 20	21, 22	23, 24
A	PC											PC
B	BLC	C5a	G-CSF	GM-CSF	CCL1	CCL11	sICAM-1	IFN-γ	IL-1α	IL-1β	IL-1ra	IL-2
C	IL-3	IL-4	IL-5	IL-6	IL-7	IL-10	IL-13	IL-12p70	IL-16	IL-17	IL-23	IL-27
D	IP-10	I-TAC	KC	M-CSF	CCL2	MCP-5	MIG	MIP-1α	MIP-1β	MIP-2	RANTES	SDF-1
E	TARC	TIMP-1	TNF-α	TREM-1								
F	PC											PBS

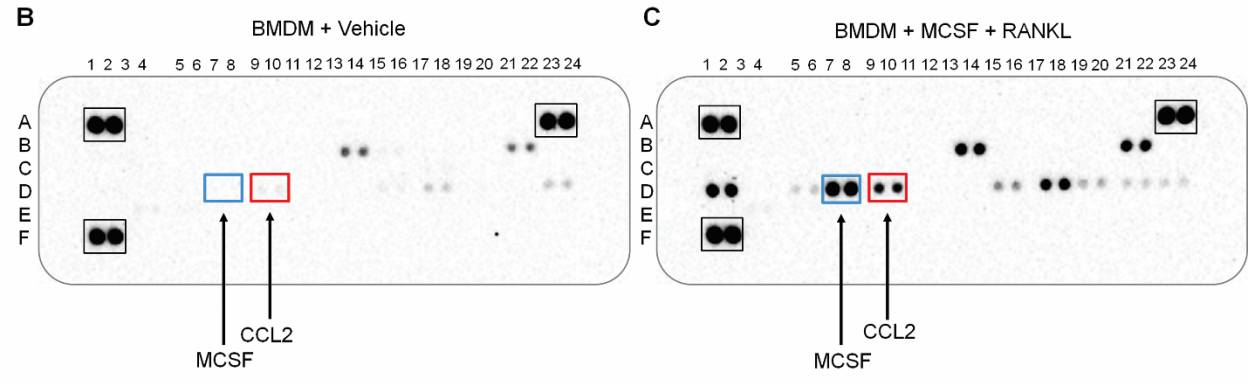

Supplementary Figure 13. Cytokine array reveals upregulation of CCL2 during osteoclast differentiation. (A) Illustration of the mouse cytokine array that includes 40 distinct cytokine/chemokine antibodies with duplicates. The array also contains three positive control (PC) proteins and one PBS negative control. (B, C) Blots after incubation with culture medium from BMDM treated with vehicle (A) or MCSF and RANKL (B) for 24 h. MCSF: 20 ng/ml; RANKL 40 ng/ml. Note upregulations of IP-10, sICAM-1, IL-1ra, MIP-1β and CCL2. Note the PC protein levels in the black boxes of the two blots are comparable. Since MCSF is added in the culture medium of (C), it could also be considered as a PC. PC, positive control; BMDM, bone marrow derived macrophage.

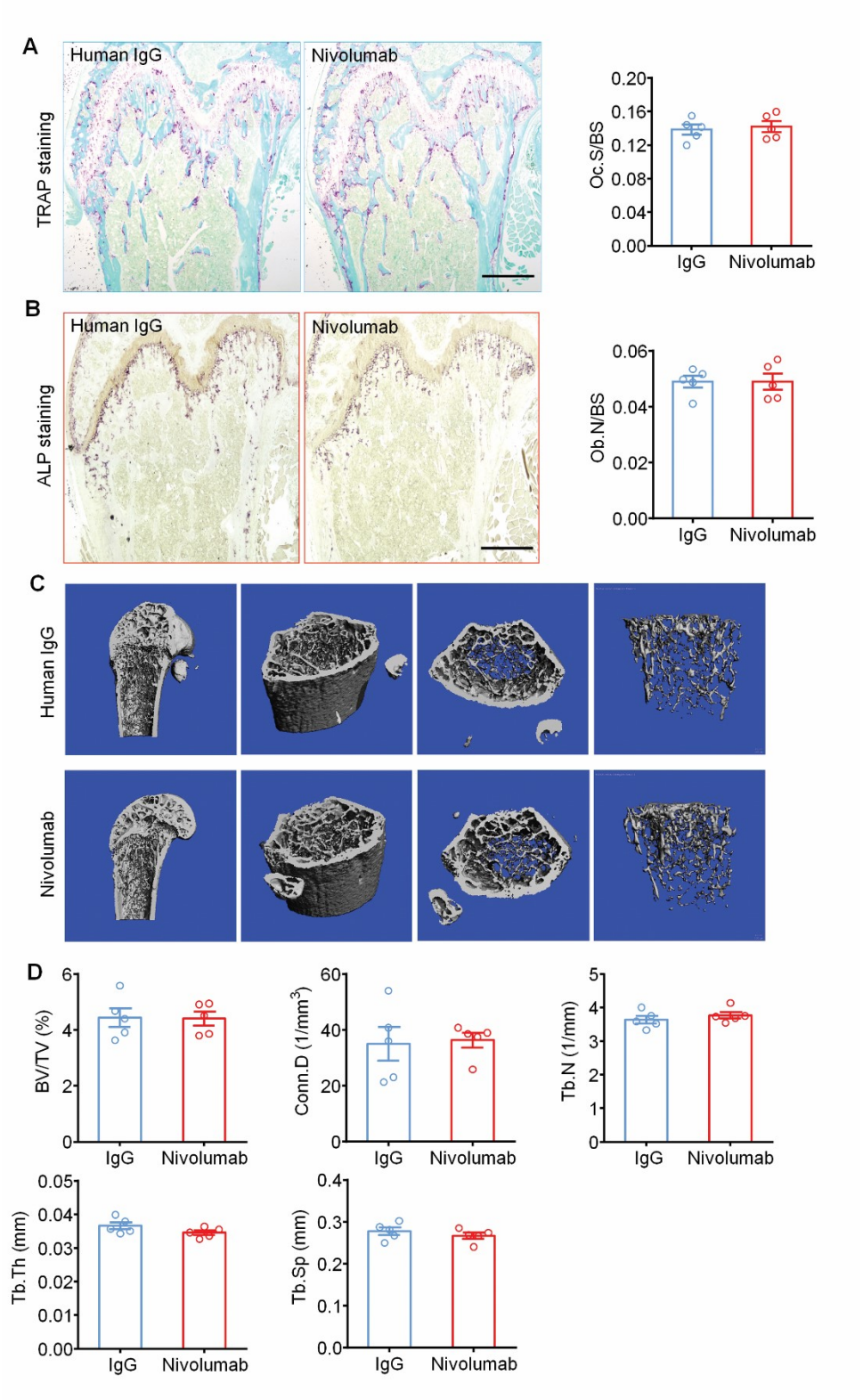

Supplementary Figure 14. Effects of human IgG or nivolumab treatment on bone

microstructure in naïve mice. (A and B) Representative images and quantification of TRAP staining (A) and ALP staining (B) showing no statistical difference between 2 groups on day 17 after treatment (5 x 10 mg/kg, i.v.). n = 5 female mice per group, and 8-10 sections were collected per femur. Scale bar, 500 μm. (C) Representative 3-dimentional reconstructed micro-CT showing bone microstructures in the distal part of femora in naïve mice receiving repeated human IgG or nivolumab treatment. (D) Comparison of morphometric parameters from micro-CT images shows no statistical difference in BV/TV, Conn.D, Tb.N, Tb.Th and Tb.Sp between human IgG treated mice and nivolumab treated mice (n = 5 female mice per group) on day 17 after treatment. Data are Mean ± SEM. Two-tailed Student's *t*-test. BL, baseline; BV/TV, bone volume/total volume; Conn.D, connectivity density; Tb.N, trabecular number; Tb.Th, trabecular thickness; Tb.Sp, trabecular separation; Oc.S/BS, Osteoclast surface per trabecular bone surface; Ob.N/BS, Osteoblast number per trabecular bone surface.

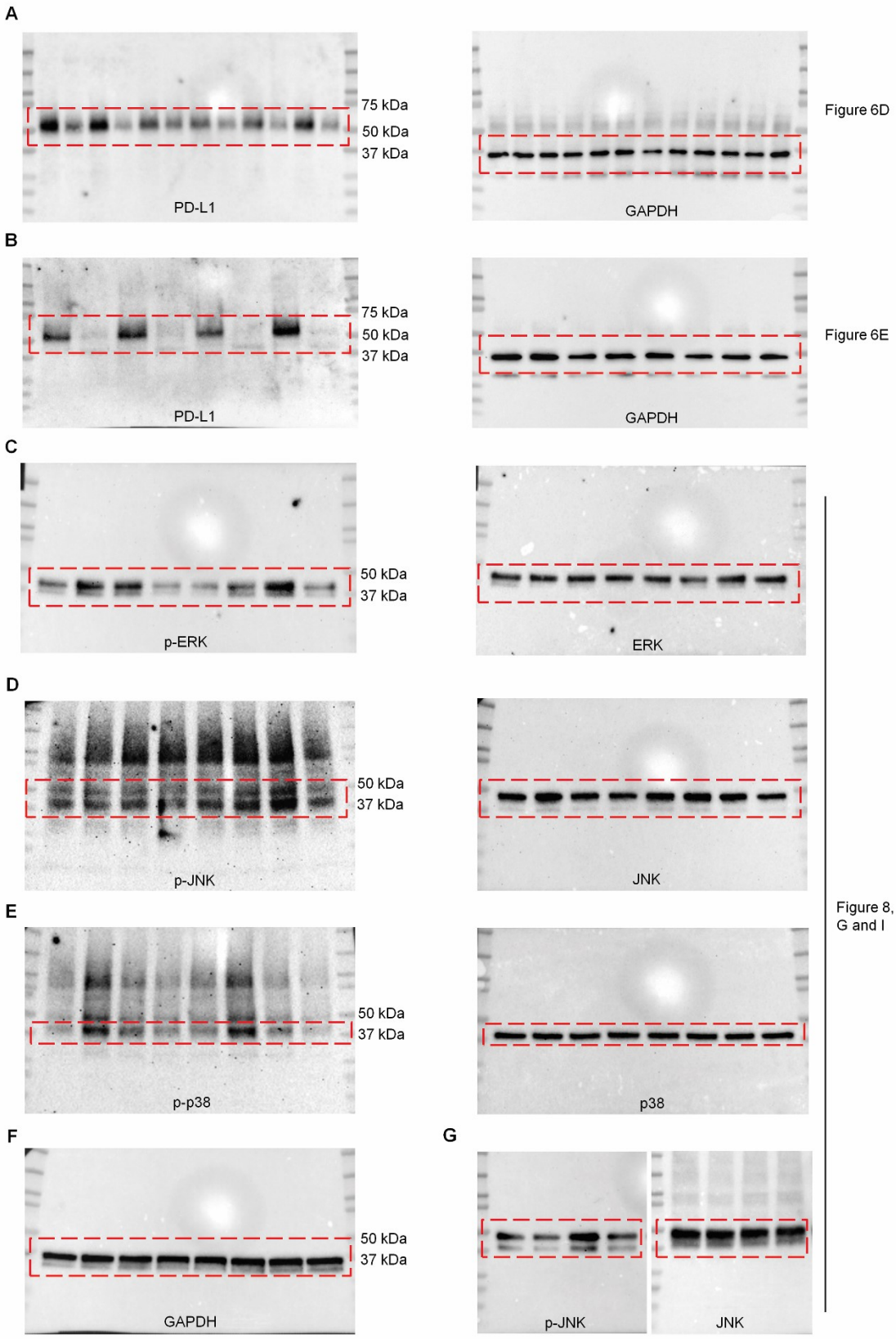

Supplementary Figure 15. Uncut gels of western blots of Figure 6 and Figure 8. (A) Full size

uncut gels of PD-L1 and GAPDH western blots for Figure 6D. (B) Full size uncut gels of PD-L1 and GAPDH western blot for Figure 6E. (C-G) Full size uncut gels of p-ERK, ERK, p-JNK, JNK, p-p38, p38 and GAPDH western blot for Figure 8, G and I.

Supplementary Table 1. Number of animals used in each figure.

Experiment	Figures	Sample size	Number of groups	Sample number	Sex	Age (weeks)	Number of animals
1. Behavioral test	Figure 2	n = 10 mice	2	20	10 male, 10 female	8-10	10 WT mice, 10 *Pd1*$^{-/-}$ mice
	Figure 4	n = 17-19 mice	2	36	20 male, 16 female	8-10	36 WT mice
	Figure 9I	n = 6 mice	3	18	10 male, 8 female	8-10	18 WT mice
	Figure S1	n = 5 mice	4 (same mice with Figure 2)	20	10 male, 10 female	8-10	10 WT mice,10 *Pd1*$^{-/-}$ mice
	Figure S2	n = 5 mice	4 (same mice with Figure 2)	20	10 male, 10 female	8-10	10 WT mice,10 *Pd1*$^{-/-}$ mice
	Figure S3	n = 8-11 mice	4 (same mice with Figure 4)	36	20 male,16 female	8-10	36 WT mice
	Figure S4	n = 8-11 mice	4 (same mice with Figure 4)	36	20 male,16 female	8-10	36 WT mice
	Figure S6B,D	n = 9 mice	2	18	10 male, 8 female	8-10	18 WT mice
	Figure S6C,E	n = 13 mice	2	26	10 male, 16 female	8-10	26 WT mice
	Figure S7	n = 11 mice	2	22	12 male, 10 female	8-10	22 WT mice
	Figure S8B	n = 10 mice	2	20	10 male, 10 female	8-10	20 WT mice
	Figure S10D	n = 7 mice	2	14	10 male, 4 female	8-10	14 *Rag1*$^{-/-}$ mice
2. Radiography and living image	Figure 1C,D	n = 10 mice	2 (same mice with Figure 2)	20	10 male, 10 female	8-10	10 WT mice, 10 *Pd1*$^{-/-}$ mice
	Figure 1F	n = 3-7 mice	4	18	male	8-10	10 WT mice, 8 *Pd1*$^{-/-}$ mice
	Figure 3C,D	n = 17-19 mice	2 (same mice with Figure 4)	36	20 male, 16 female	8-10	36 WT mice
	Figure 3F	n = 5-6 mice	2	10	male	8-10	11 WT mice
	Figure 4G	n = 8 mice	2	16	14 male, 3 female	8-10	16 WT mice
	Figure S5	n = 3 mice	2	6	male	8-10	6 WT mice
	Figure S8D,E	n = 10 mice	2 (same mice with Figure S8B)	20	10 male, 10 female	8-10	20 WT mice
	Figure S10C	n = 7 mice	2(same mice with Figure S10D)	14	10 male, 4 female	8-10	14 *Rag1*$^{-/-}$ mice
	Figure S15D	n = 5 mice	2	10	female	8-10	10 WT mice
3.Bone Histology	Figure 5B,D,F,H	n = 5-6 mice	4	20	male	8-10	16 WT mice, 5 *Pd1*$^{-/-}$ mice
	Figure 6G	n = 3 mice	1	3	male	8-10	3 WT mice
	Figure S9B,D	n = 5-6 mice	4 (same mice with Figure 5B,D,F,H)	21	male	8-10	16 WT mice, 5 *Pd1*$^{-/-}$ mice
	Figure S11B,D	n = 4 mice	2	8	male	8-10	4 WT mice, 4 *Pd1*$^{-/-}$ mice
	Figure S14A, B	n = 5 mice	2(same mice with Figure S15D)	10	female	8-10	10 WT mice
4. Flow Cytometry	Figure 6C	n = 4 mice	1	4	male	8-10	4 WT mice
	Figure 7C,D	n = 3-6 mice	3	18	6 male, 6 female	8-10	12 WT mice
5. ELISA	Figure 5I, J	n = 6-7 mice	2 (same mice from Figure 3)	13	male	8-10	13 WT mice
	Figure 6B	n = 6-7 mice	2 (same mice from Figure 3)	13	male	8-10	13 WT mice
	Figure 9A	n = 3 cultures	4	12	male	8-10	3 WT mice
	Figure 9B	n = 5-6 mice	3	17	male	8-10	11 WT mice
	Figure 9C	n = 4 cultures	4	16	male	8-10	4 WT mice
	Figure 9D	n = 4 cultures	4	16	male	8-10	4 WT mice
	Figure S5D	n = 6 mice	2	12	male	8-10	12 WT mice
6. Western blot	Figure 6D	n = 6 mice	1	6	male	8-10	6 WT mice
	Figure 6E	n = 4 mice	1	4	male	8-10	4 WT mice
	Figure 8H	n = 3-4 cultures	8	88	male	8-10	8 WT mice
	Figure 8I	n = 3 cultures	4	12	male	8-10	3 WT mice
7. In vitro TRAP staining	Figure 8D	n = 3 cultures	4	12	male	8-10	3 WT mice
	Figure 8F	n = 3 cultures	4	12	male	8-10	3 WT mice, 3 *Pd1*$^{-/-}$ mice
	Figure 8K	n = 3 cultures	4	12	male	8-10	3 WT mice
	Figure 9E	n = 3 cultures	4	12	male	8-10	3 WT mice
8. Immunostaining	Figure S12B	n = 1 cultures	6	6	male	8-10	3 WT mice
9. *In situ* hybridization	Figure 9H	n = 3 DRG	2	6	male	8-10	3 WT mice
10. Calcium image	Figure 9F	n = 23-329 neurons	3	604	2 male, 2 female	4-6	4 Advillin-GCaMP6 mice
Total number of mice							363(260 male + 103 female)

Both sexes were used. Mice shared in different experiments are underlined. A total of 363 mice were used, including 260 males and 103 females.

Supplementary Table 2. Antibodies used for flow cytometry in this study.

Antibody	Florescence	Catalog#	Company	Isotype	Dilution
F4/80	FITC	23108	Biolegend	Rat IgG2a, κ	1:200
CD3	APC/Cy7	100221	Biolegend	Rat IgG2a, κ	1:200
CD45	FITC	11-0451-82	E-bioscience	Rat IgG2b, κ	1:200
CD14	PE	301905	Biolegend	Mouse IgG1, κ	1:200
PD-L1	PE	155403	Biolegend	Rat IgG2a, λ	1:200
PD-1	Vivo-680	NDC 0003-3772-11	Bristol-Myers Squibb	human IgG1	1:1000

Experiment	Laser		405nm	488nm		633nm		Incubation
	Filter(nm)		425/50	530/30	585/42	660/20	780/60	
Monocyte	Primary Ab			CD45-FITC	CD14-PE	PD-1-680	CD3-APC cy7	30 min on ice
Macrophage	Primary Ab			F4/80-FITC		PD1-680		30 min on ice
Exosome	Primary Ab			CD90-FITC	PD-L1-PE	PD-1-680		30 min on ice